Organic Process Research & Development

Article

pubs.acs.org/OPRD

An Automated Continuous-Flow Platform for the Estimation of Multistep Reaction Kinetics

Brandon J. Reizman and Klavs F. Jensen*

Department of Chemical Engineering, Novartis Center for Continuous Manufacturing, Massachusetts Institute of Technology, Room 66-350, 77 Massachusetts Avenue, Cambridge, Massachusetts 02139, United States

Supporting Information

ABSTRACT: Automated continuous flow systems coupled with online analysis and feedback have been previously demonstrated to model and optimize chemical syntheses with little *a priori* reaction information. However, these methods have yet to address the challenge of modeling and optimizing for product yield or selectivity in a multistep reaction network, where low selectivity toward desired product formation can be encountered. Here we demonstrate an automated system capable of rapidly estimating accurate kinetic parameters for a given reaction network using maximum likelihood estimation and a *D*-optimal design of experiments. The network studied is the series−parallel nucleophilic aromatic substitution of morpholine onto 2,4-dichloropyrimidine. To improve the precision of the estimated parameters, we demonstrate the use of the automated platform first in optimization of the yield of the less kinetically favorable 2-substituted product. Then, upon isolation of the intermediates, we use the automated system with maximum *a posteriori* estimation to minimize uncertainties in the network parameters. From considering the steps of the reaction network in isolation, the kinetic parameter uncertainties are reduced by 50%, with less than 5 g of the dichloropyrimidine substrate consumed over all experiments. We conclude that isolating pathways in the multistep reaction network is important to minimizing uncertainty for low sensitivity rate parameters.

INTRODUCTION

A primary concern in pharmaceutical process chemistry is scale-up of a reaction from bench to production levels. Commonly, conditions found to be optimal at bench scale end up nonoptimal at a larger scale, due to changes in mass- and heat-transfer properties between reactor volumes. These changes in transport properties can lead to the formation of byproducts at the larger scale that were not accounted for in the preliminary optimization. In contrast to small-scale optimization followed by scale-up, it is traditionally preferred to model and parametrize a synthesis in terms of its kinetics at the small scale. The reaction kinetics are then coupled with knowledge of the effects of heat- and mass-transfer in the larger-scale reactor in order to optimize the reaction.

Continuous-flow microreactor systems have attracted much attention in the pharmaceutical industry as tools for reaction development and scale-up.[1−4] Small-scale continuous systems offer the potential for gathering significant reaction information from minimal amounts of starting material, in comparison to batch reaction development. The accelerated heat and mass transfer rates in microreactor systems further enhance the likelihood that intrinsic reaction information, such as kinetics, can be obtained and directly applied to scale-up.[5−8] Contributing to the efficiency of reaction characterization in flow is the ability to integrate online process analytics and feedback control into the continuous system.[9] Online analysis coupled with a central computer enables the potential for fully automated systems which employ smart algorithms to optimally evaluate reaction conditions and model parameters while minimizing the consumption of valuable starting materials.

Previously, we have demonstrated the application of automated, continuous-flow microreactor systems for the purposes of reaction screening,[10] optimization,[11,12] kinetic model discrimination, and kinetic parameter estimation.[13] Such systems offered the advantages of precise control of reaction conditions while minimizing both reagent consumption and user intervention. A challenge still to be considered in all of these cases is the extraction of reaction kinetic information from more complex reaction networks—those which proceed in either series or parallel and have the potential to form one or more unwanted byproducts. In this paper, we demonstrate an automated, continuous-flow system capable of both accurately estimating kinetic parameters for a series−parallel reaction network and optimizing the yield of a desired monosubstituted product. As is often the case in complex networks, however, we find that the kinetic parameters estimated by the automated system include a high degree of uncertainty—as great as 20% for some parameters—which has not arisen in automated studies of more simplified reaction networks.[13] To ensure scalability of our final results, we apply the same automated system to determining the kinetics of isolated steps in the reaction network, greatly reducing parameter uncertainties to more acceptable values of less than 4%. This yields precise kinetic estimates for all steps in the reaction pathway, including those which account for only a small amount of byproduct formation.

The model reaction network studied is the nucleophilic aromatic substitution (S_NAr) reaction of 2,4-dichloropyrimidine (**1**) and morpholine (**2**) in ethanol to form a desired 2-substituted aminopyrimidine (**4**) and the less-desired 4-substituted (**3**) and 2,4-substituted (**5**) byproducts. The

Received: July 9, 2012
Published: September 20, 2012

dx.doi.org/10.1021/op3001838 | *Org. Process Res. Dev.* 2012, 16, 1770−1782

Scheme 1. Multistep reaction network for conversion of 2,4-dichloropyrimidine to 4,4′-(2,4-pyrimidinediyl)bis-morpholine

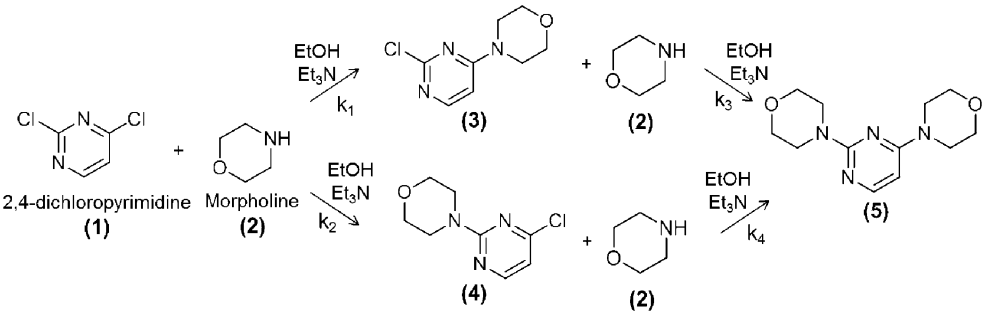

reaction network is shown in Scheme 1. As inhibitors of kinases, such as Cdks, p38, Aurora, KDR, and Gsk3, 2- and 4-substituted aminopyrimidines have generated considerable pharmaceutical interest.[14−17] The observed inhibitory effect has been attributed to hydrogen-bonding interactions between the 1-nitrogen and the 2-amino group on the pyrimidine molecule and the hinge amino acid of the kinase.[18] Synthesis of 2-aminopyrimidines is complicated by the preference of the amine nucleophile to substitute at the 4-carbon position of the substrate.[19] More aggressive reaction conditions are generally required in order to promote the second nucleophilic substitution and thereby generate the 2-amino derivative.[20,21] Using a silicon microreactor for this synthesis, we are able to safely pressurize the flow system and carry out the reaction above the atmospheric boiling point of the solvent—a traditional limitation of batch experimentation. The rapid heat-transfer rate of silicon additionally improves the likelihood of obtaining intrinsic reaction kinetics during experimentation without being limited by reaction exothermicity.

METHOD

A procedure for achieving optimal experimental design in a single-step Diels−Alder reaction has been described previously by McMullen and Jensen.[13] The procedure is iterative and can be illustrated schematically in Figure 1. Experimentation begins with an initial factorial design. On the basis of data collected through online analysis, a regression-fitting algorithm optimizes the values of parameters specified in a user-defined model in order to best agree with experimental data. Sensitivity coefficients are then calculated on the basis of the optimal parameter estimates for the experiments performed and for each candidate posterior experiment to be tested for optimality. The sensitivity coefficients are stored in the Fischer information matrix, the determinant of which gives the objective function to be minimized in the selection of a *D*-optimal posterior experiment. The optimal experiment is subsequently identified, and the prior experimental data are augmented by the results of the *D*-optimal posterior experiment. This procedure iterates until the system is terminated by a user.

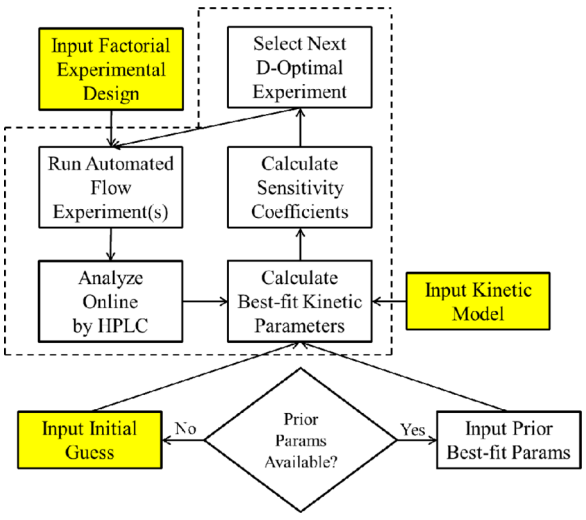

Figure 1. Logic flow diagram for automated kinetic parameter estimation in continuous flow.

Kinetic Model. We assumed for our kinetic model that all four reactions in Scheme 1 followed second-order, bimolecular reaction kinetics and that the reaction system could be modeled as an ideal plug flow reactor (PFR). The assumption of second-order, bimolecular reaction kinetics agrees with the mechanisms previously established in the literature for S_NAr reactions.[22−24] For 400-μm reactor channels and liquid-phase species diffusivities $\geq 1 \times 10^{-9}$ m^2 s^{-1}, a flow reactor can be modeled as an ideal plug flow reactor for residence times exceeding 2 min. Only small deviations from plug flow are expected for shorter reactor residence times extending down to 30 s.[25,26] We chose the minimum reaction time for our experiments to be 30 s so as not to have to deconvolute the effect of dispersion in our online kinetic analysis.

Considering our assumptions for the kinetics of the reactions in Scheme 1, we derived the following rate laws governing species generation and consumption:

$$f_1 = \frac{d(\hat{C}_u)_1}{dt} = -k_1(\hat{C}_u)_1(\hat{C}_u)_2 - k_2(\hat{C}_u)_1(\hat{C}_u)_2 \quad (1)$$

$$f_2 = \frac{d(\hat{C}_u)_2}{dt} = -k_1(\hat{C}_u)_1(\hat{C}_u)_2 - k_2(\hat{C}_u)_1(\hat{C}_u)_2 - k_3(\hat{C}_u)_3(\hat{C}_u)_2 - k_4(\hat{C}_u)_4(\hat{C}_u)_2 \quad (2)$$

$$f_3 = \frac{d(\hat{C}_u)_3}{dt} = k_1(\hat{C}_u)_1(\hat{C}_u)_2 - k_3(\hat{C}_u)_3(\hat{C}_u)_2 \quad (3)$$

$$f_4 = \frac{d(\hat{C}_u)_4}{dt} = k_2(\hat{C}_u)_1(\hat{C}_u)_2 - k_4(\hat{C}_u)_4(\hat{C}_u)_2 \quad (4)$$

$$f_5 = \frac{d(\hat{C}_u)_5}{dt} = k_3(\hat{C}_u)_3(\hat{C}_u)_2 + k_4(\hat{C}_u)_4(\hat{C}_u)_2 \quad (5)$$

The model-predicted response of species i was specified in eqs 1−5 as $(\hat{C}_u)_i$, the predicted concentration of i in experiment u

dx.doi.org/10.1021/op3001838 | Org. Process Res. Dev. 2012, 16, 1770−1782

as a function of the reaction time t, the reaction temperature T, and the initial concentrations of **1** and **2**, C_{10} and C_{20}, respectively. k_m was the rate constant for reaction m, expressed as:

$$k_m = A_m \exp\left(-\frac{E_{Am}}{RT}\right) m = 1, ..., 4 \quad (6)$$

where A_m and E_{Am} were the pre-exponential factor and activation energy associated with k_m, respectively, and R was the gas constant. To achieve better convergence to an optimal set of kinetic parameters, we defined scaled parameters θ_j such that:

$$\theta_{j=2m-1} = \ln(A_m) \quad (7)$$

$$\theta_{j=2m} = \frac{E_{Am}}{RT^*} \quad (8)$$

Equation 6 was then rewritten as:

$$k_m = \exp\left(\theta_{2m-1} - \frac{T^*}{T}\theta_{2m}\right) \quad (9)$$

where the pre-exponential factor and the activation energy were scaled comparably. We chose for our case T^* = 343 K to represent an average value for the reaction temperature in our experiments, ensuring that $T^*/T \sim 1$ over the range of reaction temperatures studied.

Approach to Parameter Estimation. The concentrations of species **1**, **3**, **4**, and **5** were measured after reaction by online HPLC. An optimal set of kinetic parameters was obtained by fitting the kinetic model of eqs 1−5 to the observed responses of **1**, **3**, **4**, and **5** as functions of T, C_{10}, C_{20}, and the residence time t_{res}. Both maximum likelihood estimation (MLE) and maximum *a posteriori* (MAP) estimation were applied in obtaining optimal least-squares regression estimates of the kinetic parameters.

For experiments in which no prior estimates for optimal kinetic parameters were available, a set of optimal kinetic parameters was found by MLE. The nonlinear programming for MLE was formulated as:

$$\min_\theta \sum_{u=1}^{N_{expt}} [C_u - \hat{C}_u(\theta)]' W_u [C_u - \hat{C}_u(\theta)] \quad (10)$$

where C_u was the $N_{resp} \times 1$ vector of measured responses for experiment u and $\hat{C}_u(\theta)$ was the $N_{resp} \times 1$ vector of model-predicted responses for experiment u with model parameters θ. W_u was a weighting matrix for the residuals which we chose to be

$$W_u = V_\varepsilon^{-1} \; u = 1, ..., N_{expt} \quad (11)$$

V_ε was the response covariance matrix, defined for species i and species j as:[27]

$$(V_\varepsilon)_{ij} = s_{ij}^2 = \sum_{u=1}^{N_{expt}} \frac{\left[(C_u)_i - (\hat{C}_u)_i\right]'\left[(C_u)_j - (\hat{C}_u)_j\right]}{N_{expt} - N_{param}} \quad (12)$$

where the difference in the number of experiments and the number of optimized parameters, $N_{expt} - N_{param}$, was strictly greater than zero. Because the objective function required V_ε as an input, we used V_ε from the previous experiment as an input to the updated MLE optimization. V_ε was initialized as the identity matrix prior to the first parameter optimization and was found experimentally to converge to a consistent set of values after only 1−2 posterior experiments. The optimization in eq 10 was performed as a constrained sequential quadratic programming (SQP) optimization in MATLAB. The lower and upper bounds on the optimization were found by computing the 98% confidence intervals on the prior optimal parameters. In order to limit online computational time, a maximum of 500 SQP iterations was allowed for the optimization.

Uncertainties in parameter values were evaluated on the basis of the parameter covariance matrix V_θ following the treatment of Beck and Arnold.[27] To calculate V_θ, we first defined the sensitivity coefficient, $(X_u)_{ip}$, for response i with respect to parameter θ_p in experiment u:

$$(X_u)_{ip} = \left.\frac{\partial(\hat{C}_u)_i}{\partial\theta_p}\right|_{\theta=\theta_{opt}} \quad (13)$$

Here θ_{opt} denoted the optimal set of MLE or MAP parameters found by SQP. Given the kinetic rate laws f_i in eqs 1−5, we were able to analytically evaluate eq 13 in the form of an ordinary differential equation:[28]

$$\frac{d(X_u)_{ip}}{dt} = \frac{\partial f_i}{\partial\theta_p} + \sum_{k=1}^{N_{resp}} \frac{\partial f_i}{\partial\hat{C}_k}(X_u)_{kp} \quad (14)$$

From the matrix of sensitivity coefficients, we calculated the Fisher information matrix, Z, which equaled the inverse of the parameter covariance matrix for the case of MLE:

$$Z = \sum_{u=1}^{N_{expt}} (X_u)' V_\varepsilon^{-1} X_u \quad (15)$$

$$Z = V_\theta^{-1} \text{ for MLE} \quad (16)$$

Estimation of the parameter covariance matrix allowed for the uncertainties of our kinetic parameter estimates to be calculated. For a single parameter θ_p, a one-dimensional confidence interval was calculated from the expression:[29]

$$\left(\theta_{opt}\right)_p - \left[(V_\theta)_{pp} t_{\alpha/2,\nu=N_{expt}-N_{param}}\right]^{1/2} \le \theta_p \le \left(\theta_{opt}\right)_p + \left[(V_\theta)_{pp} t_{\alpha/2,\nu=N_{expt}-N_{param}}\right]^{1/2} \quad (17)$$

where $t_{\alpha/2,\nu=N_{expt}-N_{param}}$ was the Student's t-distribution value for $\alpha/2$ confidence, and $N_{expt} - N_{param}$, the degrees of freedom.

The approach to MAP estimation was similar to the approach for MLE, although MAP estimation considered *a priori* estimates and uncertainties for the vector of model parameters θ. The quadratic program for MAP estimation was given as:

$$\min_\theta [\mu - \theta]' V_\mu^{-1} [\mu - \theta] + \sum_{u=1}^{N_{expt}} [C_u - \hat{C}_u(\theta)]' V_\varepsilon^{-1} [C_u - \hat{C}_u(\theta)] \quad (18)$$

where μ was the *a priori* vector of optimal model parameters and V_μ^{-1} was a weighting matrix for the difference between the prior model parameters and the optimal *a posteriori* model parameters. V_μ was identified as the *a priori* parameter covariance matrix, which could be calculated as in eqs 15 and

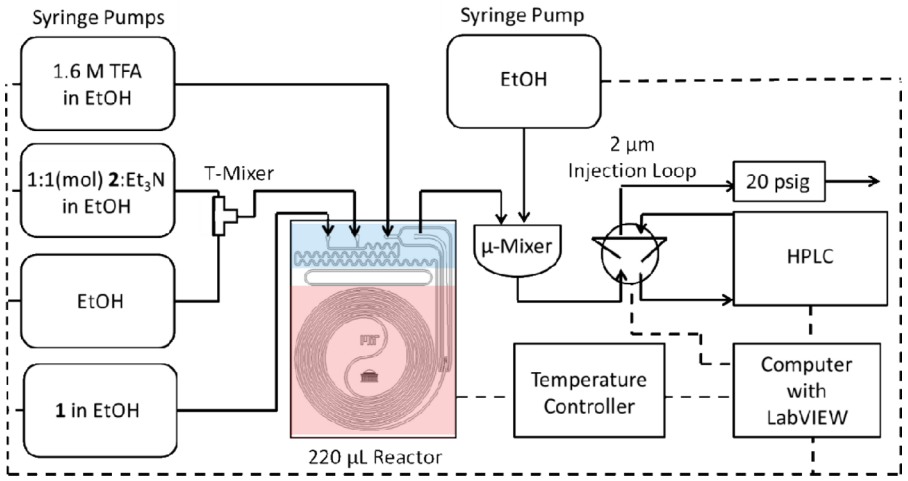

Figure 2. Diagram of the automated continuous-flow parameter estimation system.

Table 1. Experimental conditions for factorial designs

set of experiments	factorial design	levels of t_{res} (min)	levels of T (°C)	levels of equiv **2**	substrate conc (M)
initial simultaneous parameter estimation	3 × 2 × 2	0.5, 1.0, 5.0	40, 80	1.0, 2.0	0.150
isolated estimation of A_1, E_{A1}, A_2, and E_{A2}	2 × 2 × 2	0.5, 1.0	40, 100	1.0, 2.0	0.150
isolated estimation of A_3 and E_{A3}	2 × 2 × 1	10, 20	80, 100	2.5	0.050
isolated estimation of A_4 and E_{A4}	2 × 2 × 1	10, 20	80, 100	2.5	0.030
final simultaneous parameter estimation	3 × 2 × 2	0.5, 10, 20	40, 100	1.0, 2.5	0.150

16 for all prior experiments. The *a posteriori* parameter covariance matrix was then given by:

$$V_{\mathrm{MAP}}^{-1} = V_{\mu}^{-1} + V_{\theta}^{-1} \tag{19}$$

and was substituted into eq 17 for V_{θ}^{-1} in order to obtain posterior confidence intervals. The number of degrees of freedom in this case was $N_{\mathrm{prior}} + N_{\mathrm{expt}} - N_{\mathrm{param}}$, where N_{prior} was the number of prior experiments already conducted. As in MLE, the MAP optimization was evaluated in MATLAB with the constrained SQP optimization algorithm and limited to a maximum of 500 iterations.

Approach to Optimal Experimental Design. Our objective in parameter estimation was to minimize the total uncertainty and joint uncertainty in the MLE and MAP optimal parameters. Experiments were selected on the basis of the *D*-optimality criterion, introduced by Box and co-workers:[30,31]

$$\begin{aligned} D &= \min_u \left| \left(V_{\theta}^{-1} + (X_u)' V_{\varepsilon}^{-1} X_u \right)^{-1} \right| \\ \text{s.t. } u &\in \text{experimental design space} \end{aligned} \tag{20}$$

The *D*-optimal corresponded to the choice of conditions for the next experiment in the design of experiments for which the predicted volume of the parameter covariance matrix was minimized. By minimizing the volume of the parameter covariance matrix, the total joint uncertainty among all parameters in the model was minimized. For MLE, we incorporated eq 20 as written into the parameter estimation program. For MAP estimation, we substituted V_{MAP} for V_{θ} as was done for estimation of parameter confidence intervals.

Automated Parameter Estimation System. A diagram of the automated parameter estimation system is shown in Figure 2. A 0.30 M solution of **1** (98%, Aldrich, St. Louis, MO, U.S.A.) was delivered with an internal standard, 1,2-dimethoxybenzene (>99%, TCI, Portland, OR, U.S.A.) in ethanol to a silicon microreactor. A solution of 0.92 M **2** (≥99.0%, Sigma-Aldrich, St. Louis, MO, U.S.A.) and 0.92 M triethylamine (Et_3N) (≥99.0%, TCI, Portland, OR, U.S.A.) in ethanol was delivered to a T-mixer, diluted with ethanol, and delivered to the second inlet port of the microreactor. The reaction product was quenched in the quenching zone of the microreactor by a 1.6 M solution of trifluoroacetic acid (99%, Sigma-Aldrich, St. Louis, MO, U.S.A.) in ethanol. This quenched product was then further diluted to a 3:5 ratio in a micromixer by a second stream of ethanol and injected into an HPLC for online analysis. In a separate set of experiments, solutions of **3** and **4** were each reacted with a solution of 0.36 M **2** and 0.36 M triethylamine (Et_3N) to produce **5**. In the case of using **3** or **4** as a starting material, a 0.16 M solution of **3** dissolved with the internal standard in ethanol or a 0.08 M solution of **4** dissolved with the internal standard in ethanol, respectively, was substituted into the system in place of **1**. Further information regarding system design and constraints, microreactor fabrication, and online analysis can be found in the Experimental Section.

Experimental Design. The design of experiments proceeded in three stages: an initial set of experiments aimed at determining the eight parameters in eqs 1−6 simultaneously; a second set of experiments aimed at parametrizing each step of the reaction pathway in isolation; and a final set of experiments aimed at determining the eight kinetic parameters simultaneously using *a priori* estimates from the prior sets of experiments. Up to four factors were manipulated for each experiment: the reaction residence time (t_{res}), the reaction temperature (T), the initial substrate concentration (C_{i0}), and the equivalents of **2** fed to the reactor. Each set of experiments began with an initial factorial design, which characterized the effect of manipulating multiple factors upon product yield. The factorial designs have been summarized in Table 1 and are discussed in greater detail in the Supporting Information. Following the initial factorial design, experiments were chosen

dx.doi.org/10.1021/op3001838 | Org. Process Res. Dev. 2012, 16, 1770−1782

Table 2. Optimal kinetic parameter estimates and uncertainties[a] from simultaneous estimation approach

number of experiments	$\log_{10}(A_1)$	E_{A1}	$\log_{10}(A_2)$	E_{A2}	$\log_{10}(A_3)$	E_{A3}	$\log_{10}(A_4)$	E_{A4}
initial	**0.0**	**14.2**	**0.0**	**14.2**	**0.0**	**14.2**	**0.0**	**14.2**
12	3.4 ± 0.6	26.6 ± 3.2	3.3 ± 0.6	31.0 ± 3.8	−6 ± Inf[b]	52 ± Inf[b]	−2 ± Inf[b]	27 ± Inf[b]
13	3.3 ± 0.5	26.4 ± 2.7	3.3 ± 0.5	31.1 ± 2.9	11 ± 6	102 ± 43	11 ± 29	100 ± 210
14	3.2 ± 0.4	25.5 ± 2.5	3.1 ± 0.4	30.1 ± 2.8	6.2 ± 1.2	67.9 ± 8.4	3.0 ± 3.0	44 ± 22
15	3.3 ± 0.4	26.2 ± 2.4	3.2 ± 0.4	30.8 ± 2.6	6.2 ± 1.1	68.3 ± 8.2	2.1 ± 2.1	37 ± 15
16	3.3 ± 0.4	26.1 ± 2.2	3.2 ± 0.4	30.7 ± 2.4	5.8 ± 0.8	65.4 ± 5.8	2.5 ± 1.7	40 ± 12
17	3.3 ± 0.4	26.1 ± 2.1	3.2 ± 0.4	30.6 ± 2.3	5.8 ± 0.8	65.5 ± 5.5	2.4 ± 1.5	39 ± 10
18	3.3 ± 0.3	26.3 ± 1.7	3.3 ± 0.3	31.1 ± 1.9	5.9 ± 0.7	66.5 ± 5.5	2.3 ± 1.4	38.5 ± 9.6
19	3.3 ± 0.3	26.2 ± 1.6	3.2 ± 0.3	30.8 ± 1.8	6.0 ± 0.7	67.2 ± 4.9	1.8 ± 1.0	35.1 ± 6.9
20	3.3 ± 0.3	26.4 ± 1.7	3.3 ± 0.3	31.2 ± 1.9	5.8 ± 0.7	65.1 ± 5.0	2.4 ± 1.0	39.2 ± 7.0
21	3.3 ± 0.3	26.3 ± 1.7	3.3 ± 0.3	31.1 ± 1.9	5.8 ± 0.6	65.8 ± 4.0	2.4 ± 0.9	39.1 ± 6.1
22	3.3 ± 0.3	26.2 ± 1.7	3.3 ± 0.3	31.0 ± 1.9	6.0 ± 0.6	66.7 ± 4.0	2.2 ± 0.8	37.4 ± 5.8
23	3.3 ± 0.2	26.5 ± 1.5	3.3 ± 0.3	31.4 ± 1.7	6.1 ± 0.6	67.4 ± 3.9	2.1 ± 0.7	36.8 ± 5.3
24	**3.3 ± 0.2**	**26.5 ± 1.5**	**3.3 ± 0.2**	**31.4 ± 1.6**	**6.2 ± 0.6**	**68.3 ± 4.1**	**2.0 ± 0.8**	**36.0 ± 5.3**

[a]Uncertainties given as ±1 standard deviation. A_m is in M^{-1} s^{-1} and E_{Am} is in kJ mol^{-1}. [b]Inf denotes an undefined uncertainty.

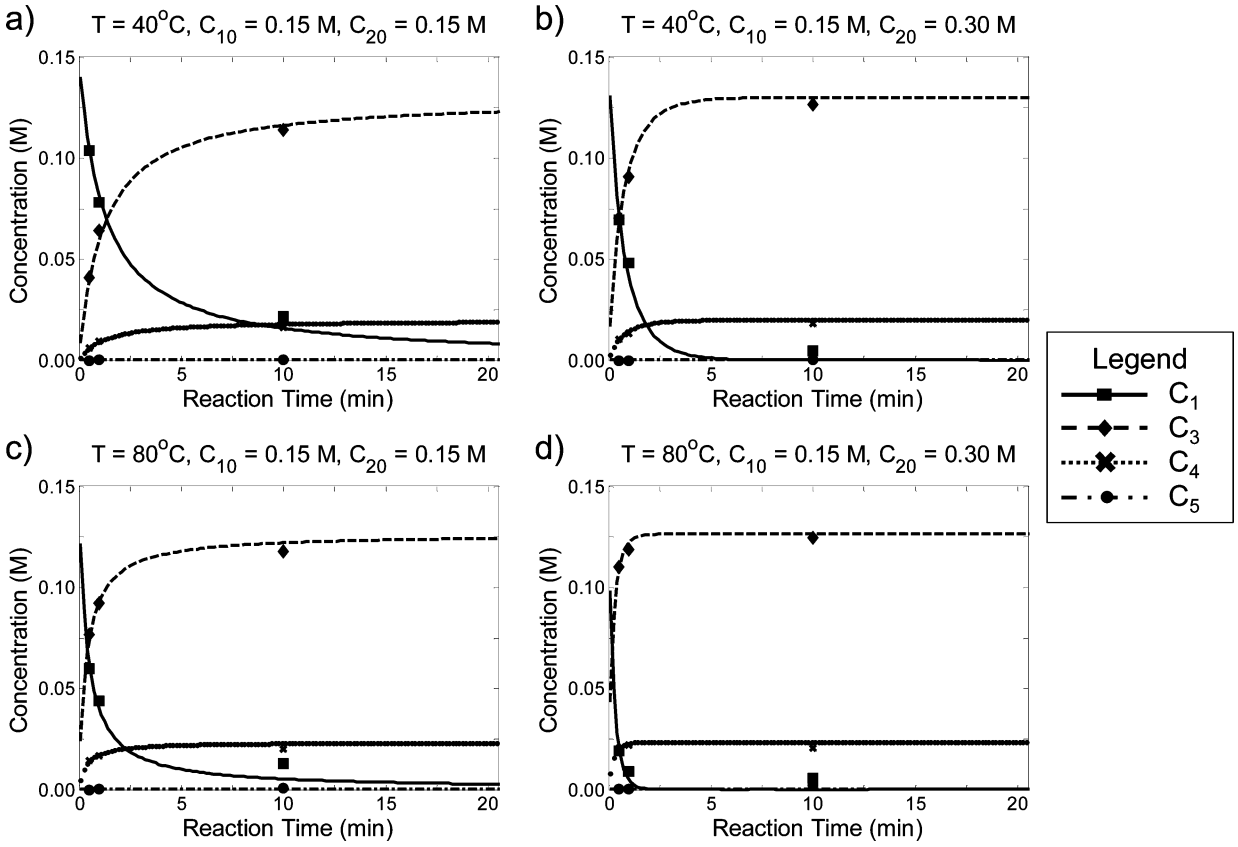

Figure 3. (a–d). Experimental and model-predicted reactant and product concentration profiles after initial factorial design (12 automated experiments). Markers identify experimental data points. Lines indicate model prediction.

sequentially from the solution of eq 20 over 1600 candidate experimental points found from enumeration of the following:

$$\begin{aligned} t_{res} &\in \{0.5\ \text{min},\ 1\ \text{min},\ 1.5\ \text{min},\ \ldots,\ 20\ \text{min}\} \\ T &\in \{40\ ^\circ\text{C},\ 60\ ^\circ\text{C},\ 80\ ^\circ\text{C},\ 100\ ^\circ\text{C}\} \\ C_{10} &\in \{0.075\text{M},\ 0.250\text{M}\} \\ \text{or } C_{30} &\in \{0.25\text{M},\ 0.050\text{M}\} \\ \text{or } C_{40} &\in \{0.015\text{M},\ 0.030\text{M}\} \\ \mathbf{2}(\text{equiv}) &\in \{0.5,\ 1.0,\ 1.5,\ 2.0,\ 2.5\} \end{aligned} \quad (21)$$

A complete list of experimental conditions tested for each experiment can be found in the Supporting Information.

RESULTS

Simultaneous Estimation of All Kinetic Parameters. Table 2 lists the best-fit parameter estimates found by MLE at the conclusion of the initial simultaneous parameter estimation factorial design. Along with each parameter estimate, the calculated uncertainty is presented as ±1 standard deviation. While estimates on the parameters relating to k_1 and k_2 show reasonable precision, the infinite uncertainties in the parameters for k_3 and k_4 imply that very little information on these

dx.doi.org/10.1021/op3001838 | Org. Process Res. Dev. 2012, 16, 1770–1782

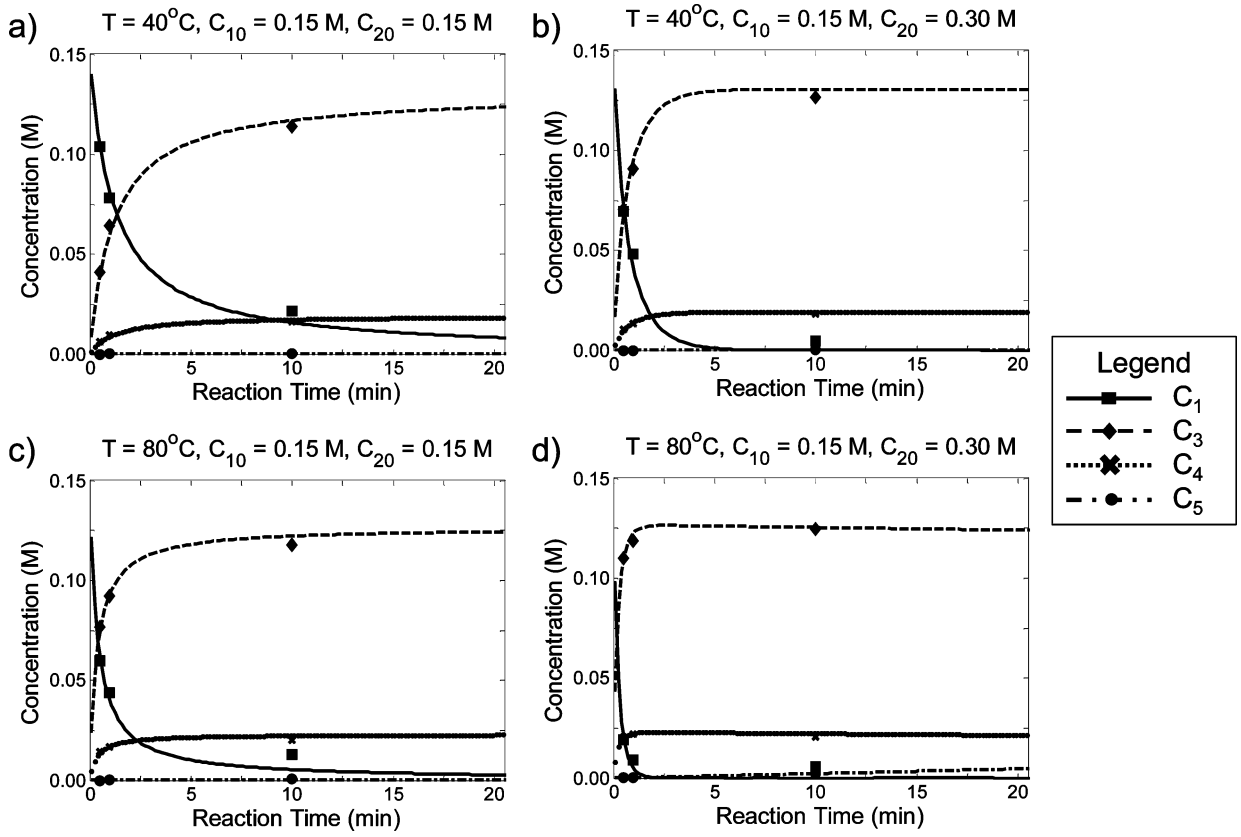

Figure 4. (a–d). Experimental and model-predicted reactant and product concentration profiles after 24 automated experiments. Markers identify experimental data points. Lines indicate model prediction.

parameters has been gathered from the results of the initial experimental design. Figure 3a–d shows the fit of the factorial design data by the initial rate parameter estimates. That the fit passes visual inspection is a testament more to the accuracy of temperature and residence time control in the microreactor system than it is to the choice of kinetic parameters. As the standard errors in Table 2 indicate, an extensive range of parameters could have been found for k_3 and k_4 which would have acceptably fit the data shown in Figure 3.

In order to minimize the uncertainty in the parameter estimates, the automated system selected the next *D*-optimal experiment to be performed at the maximum allowable residence time, temperature, concentration of **1**, and equivalents of **2**. After the collection of this data point, parameter estimates were again calculated, this time using the parameter estimates and upper and lower bounds reported in Table 2 as inputs. V_ε was also updated to agree with the covariance of the measured concentrations of the starting material and three products after the first 12 experiments. As Table 2 shows, significant improvements in the confidence of the estimates for all eight parameters were achieved after completing this first *D*-optimal experiment. In particular, uncertainties in the estimates of the pre-exponential factors and activation energies pertaining to k_3 and k_4 were all quantifiable, albeit reflective of greater than 50% error in the optimal parameter estimates.

The procedure for selecting and performing *D*-optimal experiments was repeated in an automated manner a total of 12 times (giving 24 experiments in total) before a user-specified termination. After each experiment, the initial guess for the parameter values, the bounds on the parameter values, and V_ε were updated to agree with the results of the previous parameter estimation. It is notable from Table 2 that the uncertainties in parameter estimates improve greatly after experiments 13–18, but that the uncertainties improve only modestly from experiments 19–24. The optimal parameter values also changed little for all four rate constants from experiment 18 onward. Reasoning that further experimentation would only lead to modest improvements in parameter estimates and confidence intervals, we chose to terminate the method after experiment 24 and pursue a different approach to minimizing parameter uncertainty.

Figure 4a–d illustrates the agreement between the final best-fit model parameters and experimental data after 24 experiments. The model-fit and experimental data agree well across the range of temperatures tested and at short residence times. At long residence times, the model accurately fits the yield of **5**; however, the conversion of **1** is overestimated, and the yields of **3** and **4** are underestimated. We believe this to be a consequence of the peak resolution between **1** and **3** as measured by HPLC. A high conversion generally resulted in a strong signal for **3** which, by broadening, overlapped the weak signal of **1** and reduced the accuracy of detecting and quantifying **1** at low concentrations. This claim is supported by the observation that at conditions of high conversion (temperatures at or above 80 °C, excess initial concentrations of morpholine and Et_3N), the measured conversion of **1** reproducibly reaches a maximum of 96–97% regardless of residence time. Providing that the S_NAr reaction is irreversible, it is most likely that this replicated error results from the repeated bias introduced in detecting the weak signal of **1** in close proximity to the strong **3** signal by HPLC.

dx.doi.org/10.1021/op3001838 | *Org. Process Res. Dev.* 2012, 16, 1770–1782

Scheme 2. Reaction of 2,4-dichloropyrimidine and morpholine

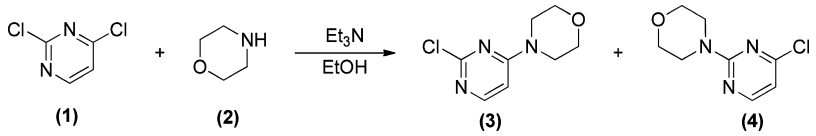

Estimation of Kinetic Parameters from Isolated Reactions. We proposed that parameter uncertainty could be reduced by decomposing the reactions in Scheme 1 into a sequence of isolated reactions. These isolated reaction steps are presented in Schemes 2, 3, and 4. The approach of isolating

Scheme 3. Reaction of 4-(2-chloro-4-pyrimidinyl)-morpholine and morpholine

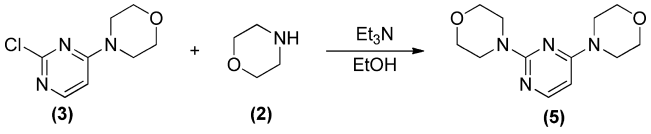

Scheme 4. Reaction of 4-(4-chloro-2-pyrimidinyl)-morpholine and morpholine

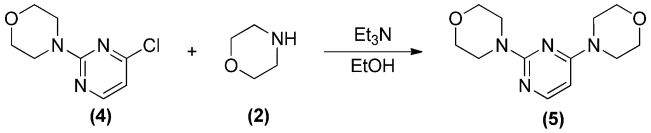

reaction steps is not uncommon to kinetic parameter estimation and may be beneficial in cases where the path through intermediates taken by the starting materials to reach the final product is unknown or ambiguous. In the case of the synthesis of **5**, we hypothesized that the large parameter uncertainties observed when attempting to estimate all eight kinetic parameters simultaneously implied an ambiguity in being able to identify whether the route from **1** to **5** went predominantly through the intermediate **3** or the intermediate **4**.

We sought first to optimize kinetic parameter estimates corresponding to k_1 and k_2 in Scheme 2. The optimization comprised a factorial design followed by four *D*-optimal experiments. MAP estimation was employed for parameter estimation, with k_3 and k_4 constrained to their prior optimal values. Table 3 demonstrates that the approach of only

Table 3. Optimal kinetic parameter estimates and uncertainties[a] from isolated estimation of parameters A_1, E_{A1}, A_2, and E_{A2}

number of experiments	$\log_{10}(A_1)$	E_{A1}	$\log_{10}(A_2)$	E_{A2}
prior	**3.3 ± 0.2**	**26.5 ± 1.5**	**3.3 ± 0.2**	**31.4 ± 1.6**
8	3.3 ± 0.2	25.9 ± 0.8	3.3 ± 0.2	31.1 ± 0.9
9	3.3 ± 0.1	26.0 ± 0.7	3.3 ± 0.1	31.3 ± 0.7
10	3.4 ± 0.1	26.6 ± 0.8	3.4 ± 0.1	31.9 ± 0.8
11	3.4 ± 0.1	27.0 ± 0.8	3.5 ± 0.1	32.2 ± 0.8
12	**3.4 ± 0.1**	**27.0 ± 0.7**	**3.5 ± 0.1**	**32.3 ± 0.7**

[a]Uncertainties given as ±1 standard deviation. A_m is in M^{-1} s^{-1}, and E_{Am} is in kJ mol^{-1}. Constrained values for parameters were $\log_{10}(A_3/M^{-1}\ s^{-1}) = 6.2$, $E_{A3} = 68.3$ kJ mol^{-1}, $\log_{10}(A_4/M^{-1}\ s^{-1}) = 2.0$, $E_{A4} = 36.0$ kJ mol^{-1}.

estimating the first four kinetic parameters resulted in rapid convergence of the parameter values and substantial reductions in uncertainties. Although the optimal kinetic parameters presented in Table 3 shifted modestly from their prior MLE values, it is important to note that the posterior optimal values in all four cases are within the prior, one standard deviation confidence intervals for each parameter found by the simultaneous parameter estimation approach. This observation would suggest that the posterior estimates of the four kinetic parameters are consistent with the results of the simultaneous parameter estimation experiment, although the posterior results have increased the likelihood that the optimal kinetic parameters are within closer proximity to the true parameter values.

A challenge often presented in complex reaction networks is the isolation of intermediate products, such as **3** and **4** in Scheme 1. We have already introduced the importance of selecting for 2-substituted pyrimidines as kinase inhibitors. In our kinetic investigation, it was similarly important to optimize for the synthesis of both the 2-substituted and the 4-substituted pyrimidines in order to isolate starting materials for the estimation of parameters in Schemes 3 and 4. Because **4** was known to be produced less favorably than **3**, we designed a synthesis which would maximize the yield of **4** at the maximum initial concentrations of **1** and **2**:

$$\max_{t_{res},T,C_{10},C_{20}} \frac{\hat{C}_4}{C_{10}}$$
$$\text{s.t. } 0.5\ \text{min} \le t_{res} \le 20\ \text{min}$$
$$40\ ^\circ\text{C} \le T \le 100\ ^\circ\text{C}$$
$$C_{10} = 0.150\text{M}$$
$$C_{20} = 0.375\text{M}$$
$$\hat{C}_1 \le 0.01(C_{10}) \qquad (22)$$

It can be derived from the proposed kinetic model that C_{10} affects the absolute concentrations of **1**, **3**, **4**, and **5** in the reaction but not the final product yields and selectivities. It followed that a greater initial concentration of **1** would allow for shorter reaction times with no adverse effect on the yield of **4**. We also found that a ridge of solution values exists for the yield optimization when C_{20} and t_{res} are allowed to vary independently. Figure 5a illustrates this ridge of optimal solutions at a temperature contour of 100 °C, where the maximum yield is 17.1%. We reasoned from this ridge of optimality that an optimum yield of **4** could be obtained in a minimum reaction time by specifying C_{20} at its upper bound of 0.375 M. Additionally, we required that our conversion of **1** exceed 99% to ensure that the starting material would not be present to complicate the isolation of products **3** and **4**.

The formulation in eq 22 generated a model-predicted optimal yield of **4** at a residence time of 49 s and a temperature of 100 °C. This optimum can be seen visually from the contour plot shown in Figure 5b. To test the predictive capability of our

dx.doi.org/10.1021/op3001838 | Org. Process Res. Dev. 2012, 16, 1770−1782

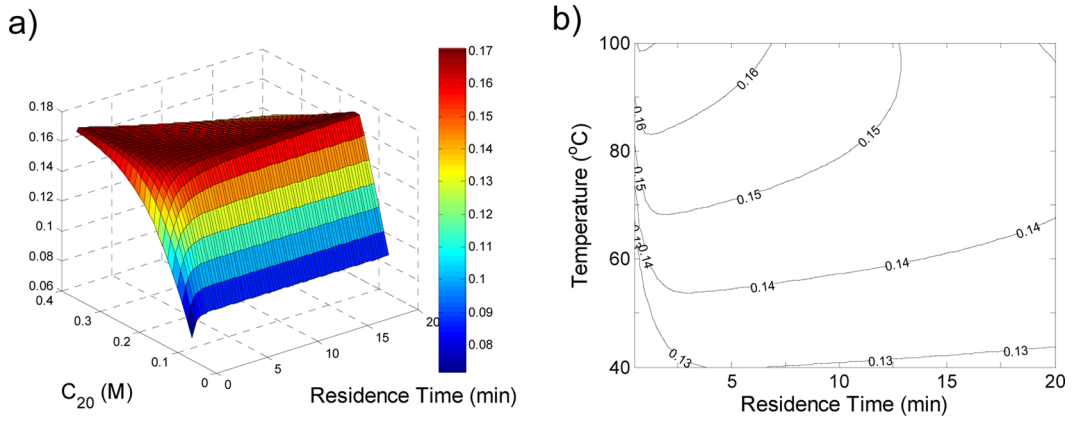

Figure 5. (a) Model-predicted yield of 4 with initial concentration C_{10} = 0.150 M and T = 100 °C based upon optimal model parameters for k_1 and k_2 from Table 3 and for k_3 and k_4 from Table 2. The ridge of maximum yield is at 17.1%. (b) Model-predicted yield of 4 with initial concentrations C_{10} = 0.150 M and C_{20} = 0.375 M based upon optimal model parameters for k_1 and k_2 from Table 3 and for k_3 and k_4 from Table 2. The maximum predicted yield is 17.1% at t_{res} = 49 s and T = 100 °C.

model, we reacted 0.745 g of **1** at the optimized reaction conditions and analyzed reactant and product concentrations by online HPLC. The experimental yields and conversion (in mass units) based upon 0.745 g of **1** are compared in Table 4 to

Table 4. Model-predicted, HPLC, and isolated yields for 1, 3, 4, and 5 for t_{res} = 49 s, T = 100°C, C_{10} = 0.150 M, and C_{20} = 0.375 M. Predictions are on the basis of 0.745 g of 1 reacted

product distribution	model-predicted[a]	measured by HPLC	isolated after workup
output **1** (g)	0.001	0.028	–[b]
output **3** (g)	0.821	0.794	0.698
output **4** (g)	0.171	0.161	0.141
output **5** (g)	0.006	0.008	–[b]
% conversion **1**	99.8	96.2	–[b]
mol/mol % yield **3**	82.2	79.5	69.9
mol/mol % yield **4**	17.1	16.1	14.1
mol/mol % yield **5**	0.5	0.6	–[b]

[a]Model predictions were calculated using optimal model parameters for k_1 and k_2 from Table 3 and for k_3 and k_4 from Table 2. [b]Workup of the product was not attempted.

the predicted yields and conversion for the optimal set of experimental conditions. It was observed that our model predictions for the yields of **4** and **5** were fairly accurate, but that our model overestimated both the conversion of **1** and the yield of **3**. Following synthesis, **3** and **4** were each isolated by column chromatography, with isolated yields reported in Table 4 in comparison to the model predictions and online HPLC analysis. Isolated yields of both compounds from workup only were between 84% and 85% and, consequently, the relative selectivity of **3** to **4** was the same for the isolated yields as was measured by online analysis.

Using the isolated product **3**, we carried out the isolated reaction in Scheme 3 to estimate the parameters for A_3 and E_{A3}. Table 5 shows that a marked convergence of the parameter confidence intervals for $\log_{10}(A_3)$ and E_{A3} was observed for the isolated conversion of **3** and **2** to **5** and that the standard errors on the estimates of the two parameters were reduced by more than 50% in the eight experiments following the four-experiment factorial design. By comparison, the final eight *D*-optimal experiments in the simultaneous estimation experiment

Table 5. Optimal kinetic parameter estimates from isolated estimation and uncertainties[a] of parameters A_3 and E_{A3} and parameters A_4 and E_{A4}

number of experiments	$\log_{10}(A_3)$	E_{A3}	$\log_{10}(A_4)$	E_{A4}
prior	**6.2 ± 0.6**	**68.3 ± 4.1**	**2.0 ± 0.8**	**36.0 ± 5.3**
4	6.2 ± 0.5	68.3 ± 3.7	2.1 ± 0.5	37.2 ± 3.1
5	6.0 ± 0.5	67.2 ± 3.5	2.2 ± 0.5	38.8 ± 3.2
6	5.8 ± 0.4	65.8 ± 2.9	2.7 ± 0.4	42.4 ± 2.5
7	5.6 ± 0.4	64.3 ± 2.9	2.7 ± 0.3	42.9 ± 2.3
8	5.3 ± 0.3	62.4 ± 2.4	2.9 ± 0.3	43.9 ± 1.9
9	5.1 ± 0.3	61.0 ± 2.3	2.8 ± 0.3	43.2 ± 2.2
10	4.9 ± 0.3	59.7 ± 1.8	2.8 ± 0.3	43.7 ± 1.9
11	4.7 ± 0.3	58.0 ± 1.9	2.8 ± 0.3	43.5 ± 1.8
12	**4.8 ± 0.2**	**59.0 ± 1.7**	**3.0 ± 0.2**	**44.7 ± 1.7**

[a]Uncertainties given as ±1 standard deviation. A_3 is in M^{-1} s^{-1} and E_{A3} is in kJ mol^{-1}.

yielded an improvement in the uncertainties of the estimates of $\log_{10}(A_3)$ and E_{A3} of less than 30%. It was also observed that the optimal parameter estimates for A_3 and E_{A3} laid outside of the 2-standard deviation *a priori* confidence interval for the individual parameter estimates. Though this would indicate an inconsistency between the simultaneous and isolated experimental data sets, we believe the reported results to be acceptable on the basis of the path taken to the new set of parameters, which remained within the 95% prior confidence intervals for A_3 and E_{A3} through the first eight experiments.

We next conducted the reaction of **4** with **2** (Scheme 4) for the estimation of A_4 and E_{A4}. Table 5 shows the convergence of the parameter estimates and single parameter confidence intervals for $\log_{10}(A_4)$ and E_{A4} over the course of 12 experiments. Both parameter standard errors improved by more than 67% from the *a priori* uncertainty values. The optimal parameter estimates for A_4 and E_{A4} were both found to be within the *a priori* 2 standard deviation single-parameter confidence intervals.

We sought upon completion of the isolated experiments to reconcile our updated set of parameters and uncertainties in a final set of MAP estimation experiments. Such experiments were necessary to account for any interaction effects between species in the reaction network and to correct for the uncertainty introduced from using lower purity chemicals in

dx.doi.org/10.1021/op3001838 | *Org. Process Res. Dev.* 2012, 16, 1770–1782

Table 6. Optimal kinetic parameter estimates and uncertainties[a] from final simultaneous experiments in isolated approach

number of experiments	$\log_{10}(A_1)$	E_{A1}	$\log_{10}(A_2)$	E_{A2}	$\log_{10}(A_3)$	E_{A3}	$\log_{10}(A_4)$	E_{A4}
prior	**3.4 ± 0.1**	**27.0 ± 0.7**	**3.5 ± 0.1**	**32.3 ± 0.7**	**4.8 ± 0.2**	**59.0 ± 1.7**	**3.0 ± 0.2**	**44.7 ± 1.7**
12	3.5 ± 0.1	27.3 ± 0.7	3.5 ± 0.1	32.1 ± 0.7	5.0 ± 0.2	60.4 ± 1.7	3.2 ± 0.2	46.3 ± 1.8
13	3.5 ± 0.1	27.1 ± 0.7	3.5 ± 0.1	32.2 ± 0.6	4.8 ± 0.2	59.0 ± 1.7	3.0 ± 0.2	45.0 ± 1.7
14	3.4 ± 0.1	27.0 ± 0.6	3.5 ± 0.1	32.2 ± 0.6	4.8 ± 0.2	59.0 ± 1.7	3.0 ± 0.2	45.0 ± 1.8
15	3.4 ± 0.1	27.0 ± 0.6	3.5 ± 0.1	32.1 ± 0.6	4.8 ± 0.2	58.9 ± 1.7	3.0 ± 0.2	45.0 ± 1.8
16	3.4 ± 0.1	27.0 ± 0.6	3.5 ± 0.1	32.1 ± 0.6	4.8 ± 0.2	58.7 ± 1.7	3.0 ± 0.2	45.0 ± 1.8
17	3.4 ± 0.1	27.0 ± 0.6	3.5 ± 0.1	32.1 ± 0.6	4.9 ± 0.2	59.4 ± 1.6	3.0 ± 0.2	45.0 ± 1.8
18	**3.4 ± 0.1**	**27.0 ± 0.6**	**3.5 ± 0.1**	**32.1 ± 0.6**	**4.9 ± 0.2**	**60.0 ± 1.6**	**3.0 ± 0.2**	**45.0 ± 1.7**

[a]Uncertainties given as ±1 standard deviation. A_m is in M^{-1} s^{-1} and E_{Am} is in kJ mol^{-1}.

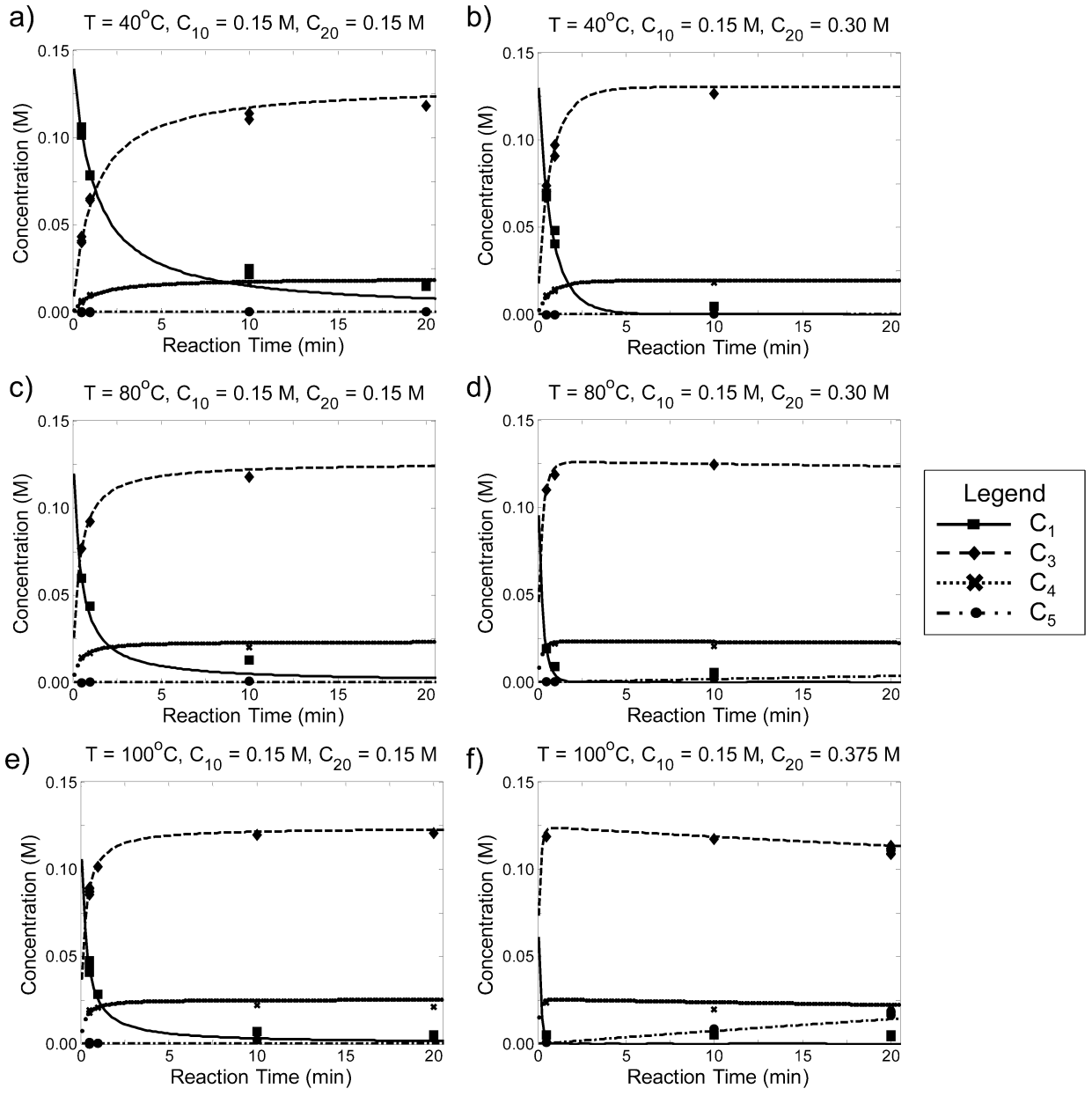

Figure 6. (a–f) Experimental and model-predicted reactant and product concentration profiles after completion of all experiments (including simultaneous and isolated approaches). Markers identify experimental data points. Solid lines indicate model prediction.

the isolated reactions of **3** and **4** with **2**. Optimizing over the same set of parameters but with the prior estimates and uncertainties found from conducting the set of isolated experiments, we were able to obtain rapid convergence of our parameter estimates with uncertainties greatly reduced over the initial simultaneous estimation approach. The convergence of the parameter estimates from experiments 12–18 of the culminating experiment are shown in Table 6. Optimal log/pre-

dx.doi.org/10.1021/op3001838 | Org. Process Res. Dev. 2012, 16, 1770–1782

exponential terms were estimated to a standard deviation of ±0.1 M^{-1} s^{-1} for k_1 and k_2 and to ±0.2 M^{-1} s^{-1} for k_3 and k_4. Likewise, standard errors for the activation energy terms were estimated as ±0.6 kJ mol^{-1} for rate constants 1 and 2 and ±1.6−1.7 kJ mol^{-1} for rate constants 3 and 4. Figure 6a−f compares the predicted concentration profiles on the basis of the optimal model parameters in comparison to the data for all experiments. The model-fit values appear to agree with the experimental data.

In total, the procedure for first simultaneously estimating kinetic parameters then isolating products and refining the kinetic parameters in isolated experimentation required 78 automated experiments to complete (with 54 experiments dedicated to estimating each kinetic parameter) and required 7 days of cumulative time. Less than 5 g of **1** were consumed for all experiments and the synthesis and isolation of **3** and **4**. A more streamlined workup and isolation routine in the future would reduce the experiment time further, as workup and stock sample preparation were the only steps carried out manually. The duration of the automated experiments was primarily determined by the time required to reach steady state for the longest residence time experiments and the rate of convergence of the system, which was a function of both the sensitivity of the experiments to the model parameters and the accuracy and precision of the continuous flow method.

DISCUSSION

The complexity of many pharmaceutical syntheses dictates that reactions be parametrized and optimized accurately and with minimal uncertainty when scaled to a production level. A large degree of uncertainty introduces the potential for inaccurate reaction scale-up, leading to lesser yields and/or increased formation of detrimental byproducts. In the initial simultaneous parameter estimation experiments, we demonstrated an automated approach that, albeit accurate, failed to reasonably minimize parameter uncertainty. The results suggested that although the model predictions in Figures 3 and 4 appeared reasonable, there could be many parameters within an error of as large as 20% yielding an acceptable fit of the experimental data. Optimizing or predictably scaling-up a system while considering these large uncertainties in kinetic parameters is infeasible.

We hypothesized from our initial results that the large uncertainties in the parameter estimates derived from the correlation in the model parameters. (For a more in depth discussion of the parameter correlation matrix describing the reaction pathway, please see the Supporting Information.) From examination of eqs 15 and 16, we identified two key factors which we expected to contribute to the correlated uncertainties between parameters. The first factor considered was the calculated response covariance V_e, which indicates the variability in both the experiment and in the measurement of the data. As continuous flow systems are excellent in their control of reaction conditions and residence time, we proposed that the variability in the experimental setup was not the major factor contributing to the large uncertainties. Alternatively, we considered the large uncertainties to be primarily a result of low parameter sensitivity across the range of experimental conditions. To address this low sensitivity, we restructured the parameter estimation so as to estimate the eight kinetic parameters from the isolated reactions in Schemes 2−4. From this restructuring, we were able to achieve significantly reduced parameter uncertainties compared to those in the simultaneous approach and confirm our notion that the originally high uncertainties resulted from low parameter sensitivity.

We suspect that the remaining parameter uncertainty after the set of posterior experiments is a combination of lower sensitivity in discriminating between the activation energy and the pre-exponential factor for each rate constant and of the inherent error in the system, estimated as V_e. From the final calculated V_e, the error in measuring **1** was found to be ±0.0064 M (±4.3% based on C_{10}), with the errors in measuring **3**, **4**, and **5** calculating to ±0.0026 M, ±0.0019 M, and ±0.0011 M, respectively. These errors can be interpreted as the limiting precision of the kinetic model, given uncertainties in flow rates, starting material purity, temperature control, and online analysis. To achieve this limiting precision, one would need to improve the sensitivity of the model to each activation energy and pre-exponential factor by conducting experiments at more extreme temperatures or by incorporating quantum calculated pre-exponential factors into the MAP estimation.

Although the parameter estimation improved substantially by analyzing isolated reactions under conditions of greater sensitivity, the method we have employed still relies upon obtaining reasonable estimates of the rate parameters in the simultaneous approach. By incorporating MAP estimation into the method, we demonstrated that the information gained from the simultaneous approach can be incorporated as *a priori* information in the isolated reaction approach to provide initial parameter estimates and to further reduce parameter uncertainty. Additionally, the optimal parameters found in the simultaneous experiment and for the isolated reaction in Scheme 2 proved to be necessary in finding conditions at which an optimal yield of **4** could be obtained.

CONCLUSIONS

The advancement of continuous flow technology with online feedback has enabled the development of automated systems capable of parametrizing and optimizing chemical syntheses with little *a priori* reaction information. For appropriate reactions and conditions, such automated systems have the potential to minimize consumption of valuable reagents while providing the requisite information for reaction scale-up. Although these systems are quite interesting for demonstration purposes, it is trivial to find cases in which the chemistry under study is too complicated to be parametrized in a handful of flow experiments. Here we have demonstrated an automated platform and procedure that are both efficient in conserving reagents and effective at parametrizing a complex reaction network.

As automated flow systems such as the one in this study continue to develop, further consideration will need to be placed upon gaining additional knowledge within the reaction system and upon designing systems with the intelligence to diagnose, model, and parametrize reaction networks without user-supplied models. To generate knowledge within the reaction system, fast online measurement tools such as flow IR will allow systems to monitor product formation near-continuously to help diagnose when and how byproduct formation occurs. The abilities to diagnose, model, and parametrize reaction networks have all been demonstrated in individual cases. As of yet, no automated system has been constructed with the intelligence to propose a novel mechanism from experimental data and to run the tests necessary to validate and parametrize that mechanism. As shown in this study, design of such a robust *a priori* system will be challenged

dx.doi.org/10.1021/op3001838 | Org. Process Res. Dev. 2012, 16, 1770−1782

by the automated system's ability to experiment at conditions of high parameter sensitivity, which often requires isolation of reactions and reaction intermediates and operation at hard-to-reach reaction conditions.

EXPERIMENTAL SECTION

System Configuration. Pumping of fluids through the microreactor and micromixer system was accomplished with the use of Harvard Apparatus PhD 2200 syringe pumps under the control of *LabVIEW* v8.6. Manipulation of pump flow rates allowed for a range of residence times and reactant concentrations to be explored. Connections downstream of the microreactor were made using 0.086 in. internal diameter PFA tubing (Upchurch Scientific, Oak Harbor, WA) to minimize dead volume. Check valves were installed on all feed streams, and a 20 psi backpressure regulator was installed downstream of the HPLC injection valve in order to dampen flow oscillations and increase the boiling temperature of the primary solvent, ethanol.

The silicon microreactor employed in this experiment was fabricated following standard photolithography and deep reactive ion etching techniques.[6] The channel cross-sectional dimensions were 500 μm (width) × 400 μm (height). A halo-etched silicon-free region of the microreactor enabled temperature control in two different zones of the reactor. At the entrance of reactants to the reactor, a 20-μL mixing zone allowed for mixing of both reactant streams at ambient temperature. The 220-μL spiral reaction zone of the reactor was then heated to a uniform temperature by a cartridge heater controlled by an Omega temperature controller to ±0.4 °C. The silicon micromixer design has been described previously[32] and allows for rapid mixing or dilution in a 4.1-μL volume. Both the microreactor and the micromixer were compression packaged to enable continuous fluid transfer throughout the system. The total volume of the system, including the microreactor, micromixer, and transfer tubing downstream of the microreactor was approximately 280 μL. To allow adequate time for the system to reach a steady state after equilibration of the reactor temperature, 1 mL of reactants was infused into the system prior to online analysis. To allow sufficient time for the syringe pumps to equilibrate, the system was additionally required to run for a minimum of 3 min at the same temperature and flow rates prior to online analysis.

On the basis of the system design, constraints were placed *a priori* upon the experimental design space. Residence times were constrained to within the range of accuracy for the syringe pumps exerting force on 5-μL glass syringes dispensing through the system under 20 psi backpressure. We estimated this range to be from flow rates of approximately 1−250 μL min^{-1} for each syringe pump. We reasoned the minimum temperature to be that at which the rate of reaction in the mixing zone of the microreactor (held at room temperature) was insignificant in comparison to the reaction rate in the reaction zone. Under this condition, the complications of the reaction mechanism in the mixing zone could be excluded from the kinetic model. A maximum temperature of 100 °C was specified so as not to exceed the boiling point of the solvent, ethanol, in the presence of 20 psi of backpressure. In future studies, a change to a higher-boiling point solvent such as *n*-butanol would enable a more extensive range of temperatures to be explored. The initial concentration of **1** was limited by the solubility of **1** in ethanol, and the range of equivalents of morpholine and Et_3N added was chosen to extend from 0.5 to 5. The number of discretizations of the experimental space (1600) was chosen to achieve an extensive range of internal points at which to evaluate the *D*-optimality condition, while at the same time limiting the time required online to exhaust all possible combinations of the four input variables.

Analyte concentrations were measured online by HPLC. Analysis by HPLC was advantageous in allowing for a quantitative separation of reaction components and demonstrated the potential for this method to be applied to more complex reaction networks. Species were measured using a Waters HPLC with 1525 binary pumps; a Nova-Pak C18 4 μm, 3.9 mm × 150 mm column; a 2996 PDA detector and Empower software. A 2-μL volume of diluted reaction product was automatically injected into the HPLC for analysis. A gradient method of water and acetonitrile was employed in order to separate **1**, **3**, **4**, **5**, and the internal standard. MATLAB code was written to integrate peak areas and determine species concentrations on the basis of previous calibrations with the internal standard. Analysis was completed in 9.25 min, at which point either reaction conditions were manipulated in preparation for collecting the next experimental data point or data were passed to the parameter estimation program in MATLAB in order to identify the next *D*-optimal experiment to conduct.

Synthesis and Isolation of Products. Products **3** and **4** were synthesized in the automated system described and are shown in Figure 2. In ethanol for 49 s at 100 °C were reacted 0.150 M **1** (corresponding to 2.0 g starting material) and 2.5 equiv each of **2** and Et_3N. The reaction product was quenched online by TFA. An aqueous extraction was performed offline to remove any salts formed from the quench of Et_3N and TFA, and the organic product was dried in Na_2SO_4. After filtration, liquid solvents were removed under vacuum to yield a white, crystalline product. This product was separated by dry loading onto 50 g of silica gel and eluting with a 4:1 solution of hexane/ethyl acetate to yield **4** in >95% purity and eluting with a 1:2 solution of hexane/ethyl acetate to yield **3** in >95% purity. HPLC yields of compounds **3** and **4** were 79.5% and 16.1%, respectively. Following workup, the isolated yield of **3** was 69.9%, and the isolated yield of **4** was 14.1%, based upon the moles of **1** reacted. The isolated compound **3** was confirmed by HPLC, IR, ^{1}H and ^{13}C NMR, and GC/MS. **4** was confirmed by HPLC, IR, ^{1}H NMR, and GC/MS. Although NMR and GC/MS cannot be used to distinguish the structures of **3** and **4**, we inferred from literature[19] that **3** was the compound produced in the greatest quantity and the compound that gave greater selectivity at low temperatures than at higher temperatures. **4** was also identified by HPLC as being notably less polar than **3**, which is consistent with the symmetric positioning of the electron-donating nitrogen atoms in the structure of **4**.

Product **5** was synthesized neat in batch in an effort to achieve a high yield in a short period of time. Such an approach was considered acceptable over a flow chemistry approach for two primary reasons. First, as the proposed kinetic mechanism suggested, the yield of **5** was maximized for arbitrarily high species concentrations and infinitely long residence times. In a case such as this, the precise control of reaction conditions afforded by a regulated microreactor system was of minimal benefit unless the reaction presented a concern for safety under uncontrolled conditions. Second, as the production of **5** under neat conditions progressed, a viscous slurry of reactants and products developed which would have been difficult to

dx.doi.org/10.1021/op3001838 | *Org. Process Res. Dev.* 2012, 16, 1770−1782

transport in our flow system without risking unsafe pressure accumulation and/or clogging of the microchannel.

Our batch synthesis of **5** began with 2.0 g of **1** reacted with 2 mL of morpholine and 3 mL of Et_3N, and the reaction yielded 3.3 g of **5** at >99% purity after 48 h at room temperature. The isolated product was confirmed by HPLC, IR, ^1H and ^{13}C NMR, and GC/MS.

Automated Calibration of Analyzed Compounds. To conserve materials and minimize the amount of manual work invested in experimental preparation, HPLC calibration curves for **1**, **3**, **4**, and **5** in relation to the internal standard were developed in an automated procedure. In the case of each calibration, a sample of the isolated reactant or product was dissolved with the internal standard into a 10-mL solution of ethanol. Each solution was then set up to be delivered via syringe pump to the micromixer, where it was to be diluted with pure ethanol and injected online into the HPLC. The automated system proceeded by manipulating flow rates of both the analyte and ethanol streams so as to generate a correlation between the HPLC absorbance signal of the reactant or product and the absorbance of the internal standard at various concentrations. We found this procedure to be effective in eliminating the effect of flow rate oscillations in the final calibration curves.

PRODUCT CHARACTERIZATION

4-(2-Chloro-4-pyrimidinyl)morpholine (3): ^1H NMR-(400 MHz, $CDCl_3$) δ 8.08 (1 H, d, J = 6.0 Hz), 6.38 (1 H, d, J = 6.0 Hz), 3.78 (4 H, t, J = 5.0 Hz), 3.65 (4 H, broad); ^{13}C NMR(100 MHz, $CDCl_3$) δ 162.8, 159.7, 155.9, 101.3, 66.5, 44.6; IR ν_{max} 2361, 1653, 1586, 1559, 1540, 1355, 1265, 1234, 1165, 1117, 979, 801 cm^{-1}; GC/MS m/z 52.0, 79.0, 114.0, 142.0, 167.9, 199.0; HPLC elution time 275−280 s, λ_{meas} = 328 nm.

4-(4-Chloro-2-pyrimidinyl)morpholine (4): ^1H NMR-(400 MHz, $CDCl_3$) δ 8.27 (1 H, d, J = 5.5 Hz), 6.64 (1 H, d, J = 5.0 Hz), 3.90−3.75 (8 H, m); IR ν_{max} 2865, 2361, 2341, 1617, 1580, 1506, 1448, 1336, 1269, 1202, 1159, 1116, 983, 962, 780 cm^{-1}; GC/MS m/z 51.9, 78.9, 113.9, 141.9, 167.9, 199.0; HPLC elution time 405−410 s, λ_{meas} = 284 nm.

4,4′-(2,4-Pyrimidinediyl)bis-morpholine (5): ^1H NMR-(300 MHz, $CDCl_3$) δ 7.96 (1 H, d, J = 6.0 Hz), 5.86 (1 H, d, J = 6.0 Hz), 3.80−3.70 (12 H, m), 3.54 (4 H, t, J = 5.0 Hz); ^{13}C NMR(75 MHz, $CDCl_3$) δ 162.8, 161.8, 157.0, 93.3, 67.1, 66.8, 44.5, 44.3; IR ν_{max} 2852, 2361, 2341, 1582, 1558, 1472, 1438, 1263, 1237, 1001 cm^{-1}; GC/MS m/z 67.1, 106.9, 134.9, 161.9, 192.8, 218.9, 249.8; HPLC elution time 180−210 s, λ_{meas} = 284 nm.

ASSOCIATED CONTENT

Supporting Information

Procedures and results for calculating the parameter correlation matrix and parameter joint confidence regions. This material is available free of charge via the Internet at http://pubs.acs.org.

AUTHOR INFORMATION

Corresponding Author

kfjensen@mit.edu

Notes

The authors declare no competing financial interest.

ACKNOWLEDGMENTS

We acknowledge the Novartis Center for Continuous Manufacturing for its generous funding of this research. We also extend great thanks to Dr. Jonathan McMullen and Jason Moore for their development of the LabView control systems for continuous flow experimentation and to Dr. Christopher Smith for his assistance in product isolation and characterization. Funding for NMR was provided by NSF Grants CHE-9808061 and DBI-9729592.

NOMENCLATURE

Symbols

A_m	Pre-exponential factor for rate constant k_m
C_{i0}	Initial concentration of species i
C_u	Measured concentration of species **1**, **3**, **4**, and **5** in experiment u
$\hat{C}_u$	Model-predicted concentration of species **1**, **3**, **4**, and **5** in experiment u
E_{Am}	Activation energy for rate constant k_m
f_i	Rate of formation for species i
i	Species index
j	Species index
k	Species index
k_m	Rate constant for reaction m
m	Reaction index
MAP	Maximum a posteriori
MLE	Maximum likelihood estimation
N_{expt}	Number of experiments
N_{param}	Number of parameters
N_{prior}	Number of prior experiments
N_{resp}	Number of measured responses
p	Parameter index
R	Gas constant (8.314 J/mol K)
S_NAr	Nucleophilic aromatic substitution
SQP	Sequential quadratic programming
s_{E_Am}	Standard error in estimation of E_{Am}
s_{ij}^2	Covariance of responses i and j
T	Reaction temperature
T^*	Scaling temperature for parameter optimization
t	Reaction time
t_{res}	Residence time
$t_{\alpha,\nu}$	Student's t value for $1-\alpha$ confidence and ν degrees of freedom
V_{MAP}	*A posteriori* parameter covariance matrix
V_ε	Response covariance matrix
V_θ	Parameter covariance matrix for optimal parameters θ
V_μ	*A priori* parameter covariance matrix
W_u	Weighting matrix for experiment u in MLE
X_u	Sensitivity coefficient matrix for experiment u
Z	Fisher information matrix

Greek Symbols

α	Confidence level
θ_{opt}	Optimal vector of model parameters
θ_p	Model parameter p
μ	*A priori* optimal model parameters

REFERENCES

(1) Hartman, R. L.; McMullen, J. P.; Jensen, K. E. *Angew. Chem., Int. Ed.* **2011**, *50*, 7502−7519.
(2) Webb, D.; Jamison, T. F. *Chem. Sci.* **2010**, *1*, 675−680.
(3) Wiles, C.; Watts, P. *Green Chem.* **2012**, *14*, 38−54.

(4) Geyer, K.; Gustafsson, T.; Seeberger, P. H. *Synlett* **2009**, 2382−2391.
(5) Hartman, R. L.; Jensen, K. F. *Lab Chip* **2009**, *9*, 2495−2507.
(6) Bedore, M. W.; Zaborenko, N.; Jensen, K. F.; Jamison, T. F. *Org. Process Res. Dev.* **2010**, *14*, 432−440.
(7) Muller, G.; Gaupp, T.; Wahl, F.; Wille, G. *Chimia* **2006**, *60*, 618−622.
(8) Watts, P.; Haswell, S. J. *Chem. Soc. Rev.* **2005**, *34*, 235−246.
(9) McMullen, J. P.; Jensen, K. F., *Annu. Rev. Anal. Chem., Vol. 3* **2010**, 3, 19-42.
(10) Goodell, J. R.; McMullen, J. P.; Zaborenko, N.; Maloney, J. R.; Ho, C. X.; Jensen, K. F.; Porco, J. A.; Beeler, A. B. *J. Org. Chem.* **2009**, *74*, 6169−6180.
(11) McMullen, J. P.; Jensen, K. F. *Org. Process Res. Dev.* **2010**, *14*, 1169−1176.
(12) McMullen, J. P.; Stone, M. T.; Buchwald, S. L.; Jensen, K. F. *Angew. Chem., Int. Ed.* **2010**, *49*, 7076−80.
(13) McMullen, J. P.; Jensen, K. F. *Org. Process Res. Dev.* **2011**, *15*, 398−407.
(14) Zhang, Q.; Liu, Y.; Gao, F.; Ding, Q.; Cho, C.; Hur, W.; Jin, Y. H.; Uno, T.; Joazeiro, C. A. P.; Gray, N. *J. Am. Chem. Soc.* **2006**, *128*, 2182−2183.
(15) Anderson, M.; Beattie, J. F.; Breault, G. A.; Breed, J.; Byth, K. F.; Culshaw, J. D.; Ellston, R. P. A.; Green, S.; Minshull, C. A.; Norman, R. A.; Pauptit, R. A.; Stanway, J.; Thomas, A. P.; Jewsbury, P. J. *Bioorg. Med. Chem. Lett.* **2003**, *13*, 3021−3026.
(16) Cumming, J. G.; McKenzie, C. L.; Bowden, S. G.; Campbell, D.; Masters, D. J.; Breed, J.; Jewsbury, P. J. *Bioorg. Med. Chem. Lett.* **2004**, *14*, 5389−5394.
(17) Tavares, F. X.; Boucheron, J. A.; Dickerson, S. H.; Griffin, R. J.; Preugschat, F.; Thomson, S. A.; Wang, T. Y.; Zhou, H. Q. *J. Med. Chem.* **2004**, *47*, 4716−4730.
(18) Wang, S. D.; Meades, C.; Wood, G.; Osnowski, A.; Anderson, S.; Yuill, R.; Thomas, M.; Mezna, M.; Jackson, W.; Midgley, C.; Griffiths, G.; Fleming, I.; Green, S.; McNae, I.; Wu, S. Y.; McInnes, C.; Zheleva, D.; Walkinshaw, M. D.; Fischer, P. M. *J. Med. Chem.* **2004**, *47*, 1662−1675.
(19) Zagulyaeva, O. A.; Bukhatkina, N. V.; Mamaev, V. P. *Zh. Org. Khim.* **1978**, *14*, 409−413.
(20) Liu, M.; Wang, S. Y.; Clampit, J. E.; Gum, R. J.; Haasch, D. L.; Rondinone, C. M.; Trevillyan, J. M.; Abad-Zapatero, C.; Fry, E. H.; Sham, H. L.; Liu, G. *Bioorg. Med. Chem. Lett.* **2007**, *17*, 668−672.
(21) Delcorona, L.; Signorelli, G.; Manzardo, S.; Pinzetta, A.; Coppi, G. *Eur. J. Med. Chem.* **1991**, *26*, 729−733.
(22) Melander, L. *Arkiv Kemi* **1950**, *2*, 211−295.
(23) Bunnett, J. F.; Zahler, R. E. *Chem. Rev.* **1951**, *49*, 273−412.
(24) Bunnett, J. F. *Q. Rev. Chem. Soc.* **1958**, *12*, 1−16.
(25) Levenspiel, O. *Chemical Reaction Engineering*, 3rd ed.; Wiley: New York, 1999.
(26) Nagy, K. D.; Shen, B.; Jamison, T. F.; Jensen, K. F. *Org. Process Res. Dev.* **2012**, *16*, 976−981.
(27) Beck, J. V.; Arnold, K. J. *Parameter Estimation in Engineering and Science*; Wiley: New York, 1977.
(28) Steinfeld, J. I., Francisco, J. S. Hase, W. L. *Chemical Kinetics and Dynamics*, 2nd ed.; Prentice Hall: Upper Saddle River, NJ, 1999.
(29) Draper, N. R.; Smith, H. *Applied Regression Analysis*; Wiley: New York, 1981.
(30) Box, G. E. P.; Draper, N. R. *Biometrika* **1965**, *52*, 355−365.
(31) Box, G. E. P.; Lucas, H. L. *Biometrika* **1959**, *46*, 77−90.
(32) Zaborenko, N.; Murphy, E. R.; Kralj, J. G.; Jensen, K. F. *Ind. Eng. Chem. Res.* **2010**, *49*, 4132−4139.